Tribology Letters, Vol. 18, No. 1, January 2005 (© 2005)
DOI: 10.1007/s11249-004-1698-2

Surface and sub-micron sub-surface evolution of Al390-T6 undergoing tribological testing under submerged lubrication conditions in the presence of CO_2 refrigerant

K.M. Lee, A.Y. Suh, N.G. Demas and A.A. Polycarpou*

Department of Mechanical and Industrial Engineering, University of Illinois at Urbana-Champaign, Urbana, IL 61801

Received 20 February 2004; accepted 13 June 2004

Carbon dioxide (CO_2) with its environmental benefits is considered a good replacement for commonly used synthetic refrigerants. In this study, the surface and sub-surface changes in simulated CO_2 environment during the initial or transient stages of a sliding contacting interface were investigated. Pin-on-disk configurations involving Al390-T6 disks in contact with 52100 steel pins were used in controlled tribological experiments using a High Pressure Tribometer. In order to evaluate the effectiveness of CO_2 refrigerant, comparative tribological experiments involving a conventional refrigerant and different commonly used lubricants were initially performed in a step-increasing load manner under submerged lubricated conditions. Subsequent detailed experiments for investigating the surface and sub-surface changes were performed in the presence of CO_2 refrigerant and the best performing lubricant, polyalkyline glycol. Burnishing was observed on the surfaces during the transient (evolutionary) stage, which indicated asperity contacts due to the breaking of the elasto-hydrodynamic lubrication film. In order to quantify the surface and sub-micron sub-surface changes that occurred during this transient stage of tribological operation, several analytical tasks were performed, which involved the measurements of nanomechanical properties, chemical compositions of the topmost 200 nm surface layer, and surface roughness. Such studies of detailed evolutionary changes that occurred during the transient stage of a tribopair shed light on the complex interactions between surface and sub-surface changes that determine whether successful tribological conditions will eventually be achieved. Based on the analyses presented in this work, it is concluded that CO_2 is a viable refrigerant from a tribology point of view.

KEY WORDS: carbon dioxide, Al390-T6, controlled tribological tests, surface roughness, nanoindentation

1. Introduction

Many engineering applications include components that experience tribological interaction that can cause significant wear or scuffing and therefore lead to malfunction or catastrophic failure. One such interaction involves the pin-on-disk found in an automotive air conditioning swash-plate compressor [1,2]. The interface is typically lubricated by a lubricant/refrigerant mixture. Normal operating conditions would involve sufficient presence of lubricant at the contact interface between the two components to resist wear and improve the mechanical performance of the compressor [2]. Fully submerged lubricated conditions can withstand extreme pressures without scuffing or failure, where scuffing is defined as the localized damage caused by the occurrence of solid-phase welding between the sliding surfaces [3,4]. It is desired to have a full film at the interface at all times to avoid direct surface-to-surface contact, which causes failure. Under favorable operating conditions, elasto-hydrodynamic lubrication (EHL) can be achieved under submerged lubrication [5]. Despite the presence of EHL conditions, fluid films can be penetrated during the early stages of the sliding contact, known as wear-in and transient periods, leading to asperity contacts. Therefore, it is crucial to understand the surface characteristics and evolutionary changes that occur at the interface from the beginning of the life of the tribological interface until a favorable "steady-state" full film EHL is reached. Such studies also shed light on the complex interactions between surface and sub-surface changes that determine whether successful EHL conditions will eventually be achieved.

In recent years, the refrigeration industry and primarily the automotive air conditioning manufacturers have shown great interest in the use of CO_2 as the refrigerant to replace harmful chlorofluorocarbon (CFC) and hydrofluorocarbon (HFC) refrigerants due to environmental concerns [6]. CO_2 is non-flammable, chemically inactive, non-toxic and inexpensive while it eliminates the need for recovery, recycling equipment and subsequent procedures, making it a good candidate for the replacement of commonly used synthetic

*To whom correspondence should be addressed.
E-mail: polycarp@uiuc.edu

refrigerants. However, there is no published research work in the open literature related to material examination, chemical analyses, and studies on the mechanical properties of surfaces in compressors that operate under the presence of CO_2.

In the present study, tribological experiments using a High Pressure Tribometer (HPT) were initially performed under fully submerged lubricated conditions with different types of refrigerant/lubricant combinations. Subsequently, fully submerged lubricated conditions with Polyalkyline Glycol (PAG) lubricant in a CO_2 refrigerant environment were simulated. This study focused on the combined effect of CO_2 refrigerant and PAG lubricant on the Al390-T6 disk/52100 steel pin interface at various stages of tribological testing to investigate the evolution of the interface before favorable EHL conditions were reached. Various analytical techniques were employed to monitor progressive evolution of this interface under submerged lubricated conditions. The performed analyses included studies of mechanical and chemical properties as well as topographical properties. The current analyses were focused on the top sub-micron layer, since no apparent change at the micro and macro scales was observed which is in agreement with the work by Pergande *et al.* [1], where changes associated with scuffing under starved lubricated conditions were limited to the surface and the topmost surface layers (~200 nm).

2. Instrumentation and controlled tribological experiments

2.1. High Pressure Tribometer

The HPT that was used to conduct the controlled tribological experiments uses a lower stationary sample in contact with an upper rotating sample. The test chamber is contained in a special pressure/vacuum housing capable of testing from 27 Pa (0.2 torr) up to 1.72 MPa (250 psi). Using a combination of heating and cooling elements, environmental chamber temperatures from −10 °C to 120 °C can be attained. The maximum normal force for the HPT is 4540 N and the maximum unidirectional rotational speed is 2000 rev/min. The HPT is equipped with computer control of the axial load and the rotational velocity of the specimen and it can measure *insitu* friction force, normal force and near-contact temperature.

The 52100 steel pin and Al390-T6 disk used in the pin-on-disk contact are materials used in actual swashplate automotive compressors. Typical sample images of a 52100 steel pin and an Al390-T6 disk used in the experiments are shown in figures 1(a) and (b), respectively. The contacting part of the pin has a dimple in the middle and is crowned with a radius of curvature of approximately 0.3 m. Figure 1(b) shows a quarter image of a typical untested (virgin) disk with clear evidence of machining marks. The samples were prescreened both optically and using a contact profilometer before initiating a test, to ensure minimal surface damage from scratches. Subsequently, the samples were immersed in a pool of acetone and ultrasonically cleaned, then rinsed with alcohol and dried using warm air.

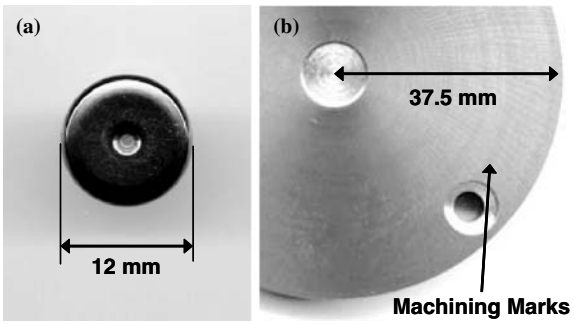

Figure 1. Typical samples used in the experiments: (a) 52100 steel pin, (b) A1390-T6 disk (quarter shown).

2.2. Tribological experiments with various refrigerants and lubricants

The properties of lubricants may significantly change depending on the refrigerants used and the operating conditions present. It has been documented in the literature that refrigerants can affect the lubricity, density, viscosity and other properties of lubricants. For example, it has been found that the properties of the PAG lubricant will be greatly affected by the CO_2 refrigerant but this is a topic currently under investigation by several researchers, e.g., [7].

In order to evaluate the effectiveness of CO_2 refrigerant against a conventional refrigerant, comparative tribological experiments were initially performed using the HPT. Different types of refrigerated conditions were simulated for controlled pin-on-disk experiments under ambient conditions (no refrigerant) and using R410a (a zeotropic mixture of difluoromethane and pentafluoroethane, each 50% by mass [1]), and CO_2 refrigerants. Furthermore, to understand the effect of the lubricant in relation to the refrigerant, two types of lubricants were employed during the experiments, namely, PAG and Polyolester (POE). Both PAG and POE lubricants had the same viscosity (ISO VG 46). Furthermore, the PAG lubricant used in these experiments was an end-capped lubricant whose properties are summarized in table 1 [8].

The contacting interface between the test specimens was submerged in the lubricant while the environmental chamber, after being evacuated, was pressurized in the presence of refrigerant to a certain chamber pressure corresponding to the operating pressure in a compressor. Specifically, the chamber pressures were set to

Table 1.
Properties of end-capped PAG lubricant [8].

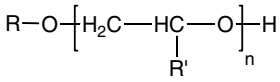

Density @ 15 °C	Pour Point, ASTM D 97 (°C)	Flash Point, COC (°C)	Viscosity, ASTM D 445		Viscosity Index, ASTM D 2270
			40 °C (cSt)	100 °C (cSt)	
1.007	< −40	234	44.5	9.8	215

1.4 MPa (200 psi) for the tests with CO_2 and 0.34 MPa (50 psi) for those with R410a. The linear speed was set at 2.4 m/s while the controlled temperature in the chamber was set at 90 °C. A series of tests were performed with different refrigerant/lubricant combinations employing a method of incremental loading. A typical experiment is shown in figure 2 where the applied normal force, friction coefficient and near-contact temperature are plotted in terms of test duration. An initial normal force of 227 N with a step increase of 454 N every 2.5 min was used and the test durations were 25 min for all experiments. Near-contact temperature was measured using a miniature thermocouple inserted in the pin at 2 mm below the contact surface.

Optical images of the disks tested under different refrigerant and ambient air conditions are shown in figure 3, for which PAG lubricant was used. From visual inspection, the disk surface shown in figure 3(a) (CO_2 refrigerant) exhibits a mild burnishing track approximately 8 mm in width. On the other hand, relatively severe burnishing marks were present on the disk surfaces tested with R410a refrigerant and ambient air, shown in figure 3(b) and (c), respectively. These disks exhibit two distinct burnishing bands separated approximately by 8 mm in width. These bands that appear within the track correspond to locations of maximum contact pressure for the crown geometry of the pin (figure 1(a)). From visual observation, it was deduced that the disk tested with CO_2 refrigerant experienced less burnishing than those tested with R410a refrigerant or ambient environment, hence indicating better performance. Note that in all cases no visible wear was seen on the much harder and smoother 52100 steel shoes.

In an attempt to quantify the burnishing on the tribologically tested disks, long profilometric scans were measured across the burnishing tracks using a contact profilometer. The measurements are depicted in figure 4. As expected, in the case of CO_2 refrigerant, figure 4(a) shows only minor burnishing ($\sim$0.2 μm) and the absence of severe burnishing marks, in agreement with the optical image of figure 3(a). On the other hand, the measurements shown in figure 4(b) and (c) exhibit distinct bands corresponding to the two relatively "severe" burnishing tracks, which are approximately 0.5 μm deep in both cases. It is, however, worth noting that the amount of burnishing is comparably small in all cases relative to the original machining marks. This is better seen in figure 5 where it shows a Scanning Electron Microscopy (SEM) image of the burnishing track on

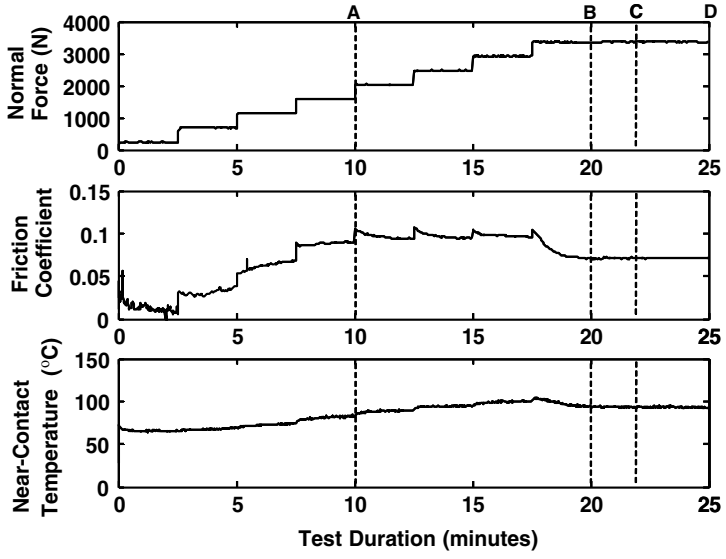

Figure 2. Typical experiments under submerged lubricated conditions using PAG lubricant in a CO_2 environment.

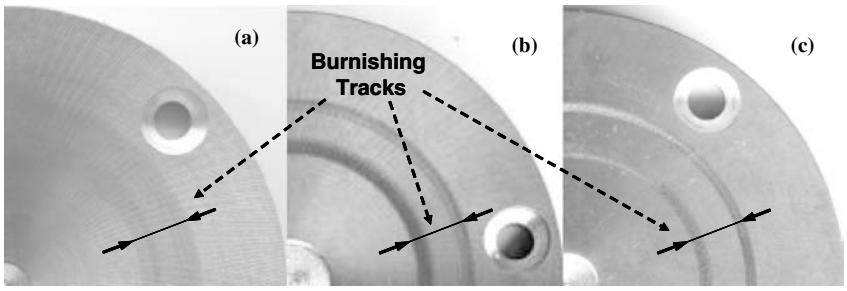

Figure 3. Optical images of disks tribologically tested using refrigerant and lubricant combination of (a) CO_2 and PAG, (b) R410a and PAG and (c) ambient air and PAG.

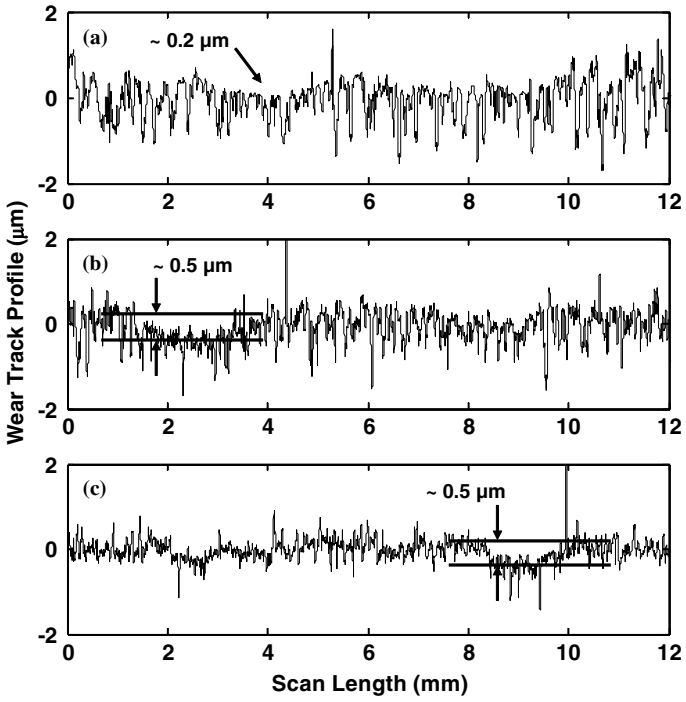

Figure 4. Surface long profile measurements across the burnishing tracks of disks tested with (a) CO_2 and PAG, (b) R410a and PAG and (c) ambient air and PAG.

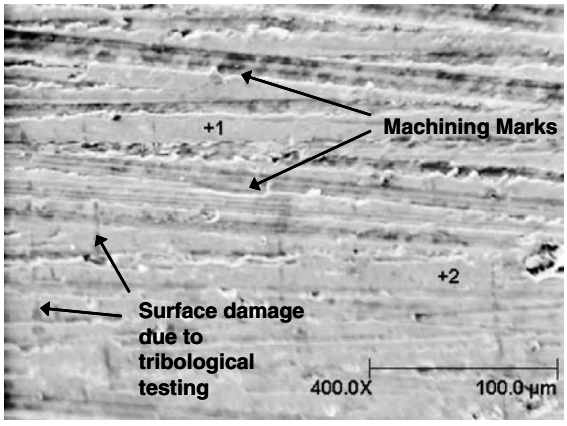

Figure 5. SEM image of sample C ($t = 22$ min, see table 3).

the disk tested with PAG and CO_2 for 22 min (sample C, see table 2). Although burnishing marks were evident on the disk surfaces, machining textures were more predominant.

Following the same test protocol described above, experiments were repeated using POE lubricant with CO_2. Based on these experiments, it was observed that CO_2 performed better than R410a. Since R410a refrigerant and air did not perform as well with the PAG lubricant in the previous set of experiments, they were not repeated with the POE lubricant. Interestingly, both visual inspection and profilometer measurements showed that POE/CO_2 combination did not result in significant burnishing on the disk surface similar to what was observed in the PAG/CO_2 combination. Note that while the quantitative difference in disk burnishing due to PAG and POE was minor under CO_2

Table 2.
Disk samples summary for experiments under CO_2/PAG environment.

	Description	Testing time	Maximum load
Virgin Sample	Unaffected part of disk	0 min	0 N
Sample A	Worn part of disk	10 min	1560 N
Sample B	Worn part of disk	20 min	3340 N
Sample C	Worn part of disk	22 min	3340 N
Sample D	Worn part of disk	25 min	3340 N

environment, there was a significant disparity in the pin wear after the experiments. The steel pin surface tested with POE showed relatively severe and distinct wear scars, whereas the burnishing on the pin surface tested with PAG was untraceable with the profilometric measurements.

These findings are in agreement with Li *et al.* [9], where they investigated the performance of various lubricant chemistries with CO_2. While they concluded that lubricant choice would depend on the application, it was documented that PAG presents fewer disadvantages than POE. Furthermore, it has been reported that PAG has better lubricity for CO_2 applications [7]. Therefore, for the remainder of this study, PAG was chosen as the primary lubricant to be used in the pin-on-disk tribological tests performed in CO_2 refrigerated environment. In the following section, controlled tribological experiments using CO_2/PAG under different stress conditions are discussed in further detail.

2.3. Controlled tribological experiments using CO_2 and PAG

A series of tests were performed with different maximum normal loads and test durations to quantify the evolutionary nature of the contacting interface under CO_2/PAG environment. For each experiment, progressively higher normal loads were imposed at four selected time durations as a means to study the evolutionary change in the sample as it goes through transient stage before reaching stable EHL conditions. The disk samples corresponding to each test are summarized in table 2 and the different time durations are marked for each of the experiments as A (10 min), B (20 min), C (22 min) and D (25 min) as also shown in figure 2. Note that each experiment under the given testing conditions was repeated three times to ensure repeatability.

The loading pattern was the same for all samples except for samples C and D for which there was no increase after 20 min due to instrument limitations. During these experiments, as expected, the coefficient of friction remained low, always being less than 0.1, while there was minimal burnishing on the disks despite the high normal forces and long time durations of these experiments. A somewhat higher fluctuation, however, was seen during the first few minutes of testing, corresponding to mild wear-in process, due to the small normal load applied (227 N). The friction coefficient increased slightly with higher normal loads as seen from 5 to 18 min. Beyond this point, which corresponds to a normal force of 3340 N, a stable friction coefficient value was reached, implying that some kind of steady-state operation was reached. Similarly, the near-contact temperature always remained low to less than 100 °C due to the presence of EHL conditions.

The presence of full film conditions after the transient period was confirmed with additional experiments under identical conditions as sample D, but run for over 60 min. In these tests, the friction coefficient and near-contact temperature remained constant after the initial transient period without failing and without the evidence of severe wear or scuffing, suggesting the formation of stable EHL conditions. Once the high asperity peaks were burnished off and the oxide layers were successfully formed, stable EHL was achieved, thus completely separating the surfaces and preventing further asperity contacts. To check for the existence of EHL lubrication, simple smooth surface EHL theory [5] was used to calculate the minimum film thickness at the pin-on-disk interface. Based on simple point contact geometry, it was found that the minimum thickness of the lubricant film was 1–2 μm. Compared to three times the root-mean-square (RMS) value of the virgin disk roughness ($S_q = 0.522$–0.813 μm, see section 5 and table 2 for details), it is suggested that the EHL film is initially penetrated allowing asperity contacts between the surfaces which leads to burnishing. However, as the burnishing progresses on the disk surfaces, the EHL thickness eventually surpasses the disk roughness (i.e., $3 \times$ RMS), leading to a somewhat stable EHL film.

3. Nano-scale mechanical properties of Al390-T6 disks

It is known that the tribological behavior of materials depends on their mechanical properties. For instance, while the wear process of a material is greatly affected by its hardness, hardness itself can change during the life of a tribopair. However, while gross hardness in bulk material is often not affected by mild wear, hardness of the topmost surface layers can be

significantly altered. In this study, Vickers hardness measurements were performed on each sample at normal loads corresponding to residual indentation depths of 8–17 μm. It was found that statistically there was no difference in hardness values among the samples. This shows that the layer below the topmost surface at the sub-micron scale was not affected, which was in agreement with the scuffing experiments on Al390-T6 by Pergande *et al.* [1]. Therefore, it is important to accurately measure and monitor the properties of the topmost surface at the nanometer scale as the disk undergoes various stages of tribological exposure.

A technique known as nanoindentation proposed by Oliver and Pharr [10] can be used to measure the mechanical properties of reduced elastic modulus and hardness of thin films and layers for depth scales varying from nanometers to sub-micrometers [11,12]. Despite the difficulties associated with nanoindentation measurements on rough engineering surfaces, experimental work by Pergande *et al.* [1] has shown that nanoindentation can successfully be performed on engineering samples using statistical analysis to extract meaningful properties. In this work, nanoindentation experiments were performed to quantify the evolution of hardness in the 200 nm topmost layer. The data were analyzed using statistical techniques of confidence intervals for mean response.

3.1. Sample preparation and instrument used for nanoindentation

The tested disks were sectioned with electrical discharge machining (EDM) in order to prevent residual stress build-up in the samples. Five slices of disk samples (virgin part and samples A through D) were individually cut across the width of burnishing track into small specimens with approximate dimensions of 10 mm × 7 mm × 3 mm. The experiments were directly performed on the tribologically tested surfaces in order to quantify the progressive changes of the topmost surface layers.

Two different types of indenter tips were used to indent the surfaces for different contact depth ranges. Contact depth is the vertical distance along which contact between indenter and surface is made [10]. In this study, a 90° cube corner indenter was calibrated for contact depth from 5 nm to 45 nm and a Berkovich indenter was calibrated from 40 nm to 200 nm.

3.2. Nanoindentation results and discussion

Although both reduced elastic modulus and hardness values were obtained from the nanoindentation experiments, only the latter were analyzed in this study since the modulus data were not affected by the testing, in agreement with Pergande *et al.* [1]. The hardness values of the samples were plotted versus contact depth for both indenters, and trend lines were drawn using a least square method. An example of these data is shown in figure 6, where it depicts extracted hardness values for sample A with statistical trend lines. For all the samples it was observed that the hardness values exhibited a larger gradient for the topmost surface layer up to 55 nm, and the variation of hardness decreased significantly for deeper contact depths. The 50 nm thick surface hardening is primarily due to the presence of oxides and in this particular case silicon oxide rich tribolayer that forms on the surface, and is further discussed in Section 4.2. Based on the hardness values gradient, the statistical studies were performed separately for two ranges of contact depths, namely 0–55 nm and 55–200 nm. It should be noted that these ranges do not exactly correspond to the calibration ranges mentioned above for the two indenters, which implies that the change in hardness slope was not caused by the choice of indenter. The transition of the hardness trends at 55 nm occurred according to indentation depths and was not affected by the type of indenter. Also drawn in figure 6 are the 95% confidence interval lines and 95% prediction interval lines [13]. A confidence interval defines a band, which has a certain probability of containing the true sample mean and a prediction interval defines a band that has a certain probability of containing a single new event.

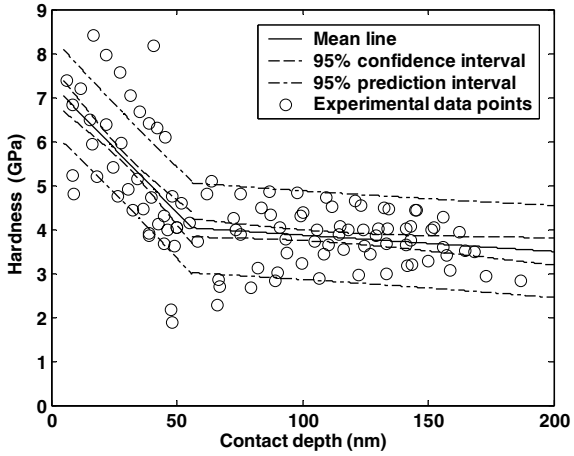

Figure 6. Statistical analysis of hardness vs. contact depth for sample A ($t = 10$ min).

To clearly establish the trends in the data, the mean hardness values and their 95% confidence intervals for virgin sample, samples A and D are plotted in figure 7 at various contact depths (for clarity reasons only 6 discrete contact depths are depicted). It was shown that sample A was harder than the virgin sample for all contact depths and sample D was softer than sample A. The difference between the samples, especially virgin and sample D, decreased as the contact depth increased, which implied that the changes in hardness due to tribological testing under submerged lubrication

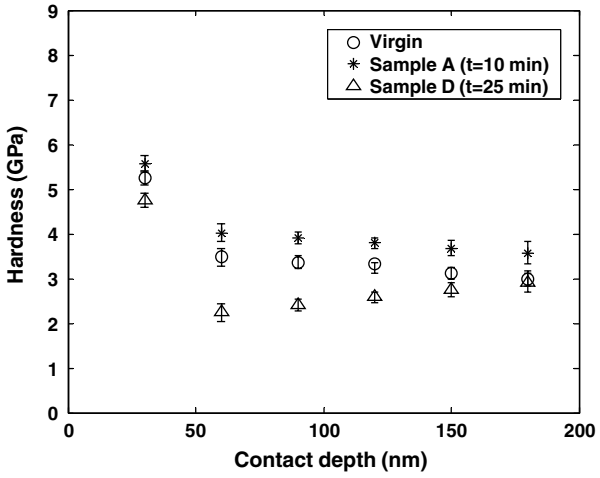

Figure 7. Mean hardness values at discrete contact depths with 95% confidence intervals.

conditions were limited only to a very thin topmost surface layer. Note that the difference between virgin and sample A is larger than that between virgin and sample D at deeper contact depths.

Based on these results, it was seen that the hardness of Al390-T6 disks increased during the initial stages of transient behavior, and decreased with progressive tribological testing during the transient stages. However, the hardness values of virgin and sample D determined by contact depths deeper than 150 nm were similar, which implied that only the very thin topmost surface layer was affected by the tribological testing as it approached the end of the transient stage considered in this study ($t = 25$ min). These variations in hardness were confirmed by chemical (section 4) and topographical (section 5) analyses.

4. Nano-scale surface and sub-surface chemical analysis of Al390-T6 disks

It was shown in the previous section that the tribological testing performed under submerged lubricated conditions caused changes in the mechanical properties of the topmost surface. To further verify the surface and sub-surface evolution, changes in chemical composition were also investigated. Generally, wear generated by sliding contact between two components leads to the removal of the topmost surface layers and also some material transfer between the two surfaces, leading to changes in chemical compositions. Previous experimental studies on the mechanism of wear and scuffing confirmed the existence of "mixed" surface layers of the order of few hundreds of nanometers [1].

Changes in chemical composition during submerged tests were investigated in the top 200 nm of the Al390-T6 disks using the Auger Electron Spectroscopy (AES) depth profiling method [14]. Based on the sample materials and testing conditions, four major chemical elements were specifically sought during the AES analysis. The main atomic components of interest were carbon, oxygen, aluminum, and silicon. The objective of this analysis was to investigate the change in each atomic concentration as burnishing on the Al390-T6 disk surface progressed under submerged lubrication.

4.1. AES experimental details

The samples used for the AES experiments were similar to those used for nanoindentation. Since any surface contaminants resting on the sample surfaces may adversely affect the AES sputtering process, each specimen was ultrasonically cleaned in acetone and rinsed off with ethanol. The calibrated sputter rates were chosen to be 24 nm/min for samples A, B, and C, and 30.5 nm/min and 17.0 nm/min for the virgin sample and sample D, respectively. Sputter durations were chosen to yield sub-surface depths ranging from 0 to 200 nm for all samples. Note that due to the dominant machining marks, the disk surfaces observed under the SEM were rough and highly directional, as seen in figure 5. Since significant roughness on the surfaces may interfere with the sputtering process, relatively smooth local areas were chosen as the sputtering (analysis) sites. Two such points (designated as 1 and 2 in figure 5) were selected for each disk and the data were examined for variability.

4.2. AES results and discussion

The locations selected within each sample showed similar trends; hence only one AES sputtered point was presented in this study. The concentration values plotted on the ordinate of figures 8 and 9 are the averaged values in the top 20 Å layer. Note that 0 nm refers to the top surface where the sputtering process starts, and the positive depth profile refers to the depth below the surface.

As shown in figure 8(a), the virgin surface exhibited a fast increase in aluminum concentration (from zero concentration) with increasing depth below the surface, reaching a steady-state value of 90% at approximately 30 nm below the surface. On the other hand, both the carbon and oxygen elements, which initially displayed high atomic concentrations, decreased to steady-state values of about 3% at 20 nm and 30 nm, respectively. The initial existence of relatively high concentration of oxygen ($\sim$70% at 3 nm) indicated the existence of an oxide layer that was present in the topmost surface as a result of oxidation due to exposure in ambient environment. The initial peak in oxygen concentration was consistent with those seen in similar studies [15]. The silicon concentration also increased from zero, but remained low at approximately 3% for the rest of the depth range considered. Note that the

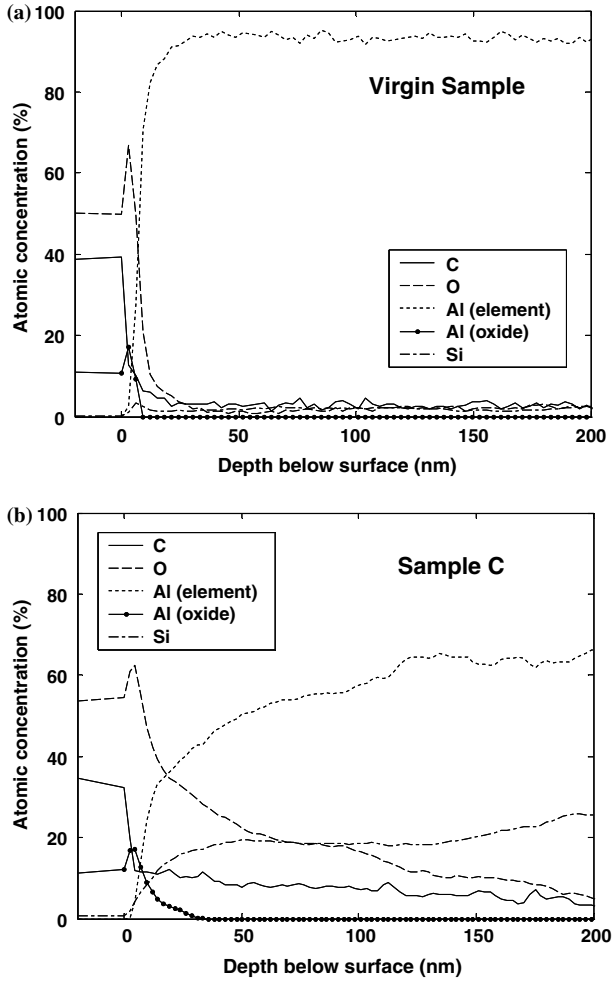

Figure 8. Percent atomic concentration on (a) virgin sample and (b) sample C ($t = 22$ min).

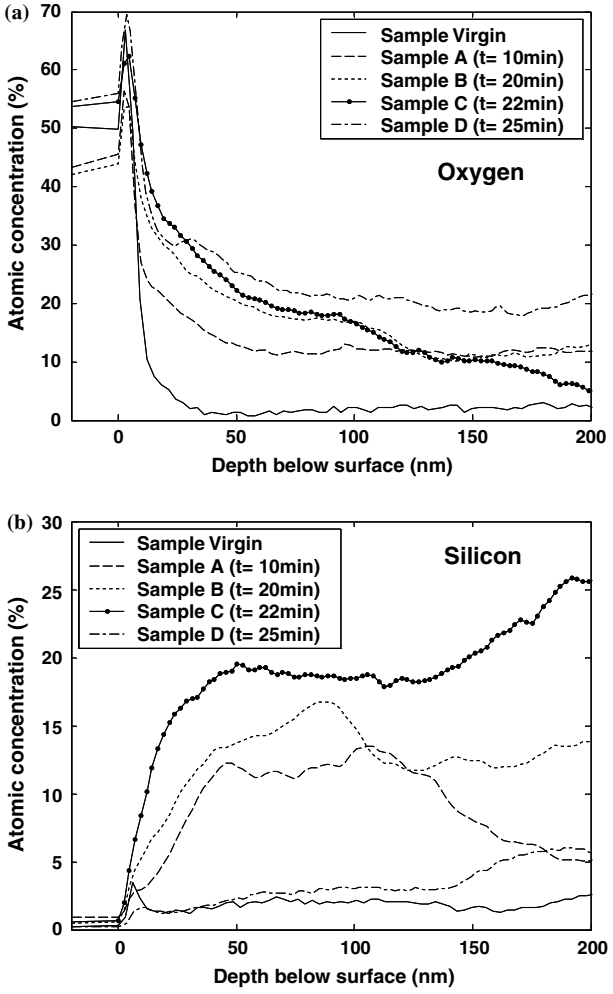

Figure 9. Variation in concentration with progressive burnishing for (a) oxygen and (b) silicon.

silicon concentration of the topmost mixed layer is different from the total silicon content in the bulk matrix of Al390-T6 (see table 3). While silicon exists as particles with sizes ranging from microns to tens of microns in the bulk matrix, this is not the case in the topmost mixed layer, which was only few hundreds of nanometers thick [1].

On the other hand, drastic changes were observed in the individual atomic concentrations of the worn samples as depicted in figure 8(b). In all of the worn samples the aluminum concentration did not display a fast rise to a steady-state level as in the case of the virgin sample. The depth profile for samples A through D showed relatively slow increase in aluminum concentration with depth below the surface, reaching 60–80% of the total concentration at 200 nm. Similarly, there were much higher concentrations of oxygen, carbon, and silicon as tribotesting progressed. The elemental concentration changes are better seen in figures 9(a) and (b) where the atomic concentrations of oxygen and silicon are plotted, respectively, as a function of depth blow the surface for all samples. Figure 9(a) depicts a monotonic increase in the concentration of oxygen in the worn sample compared to the virgin sample. All the data consistently displayed high initial peaks at shallow depths, which suggested the presence of a unique oxide layer within which the oxygen concentration was at its maximum. The high hardness values observed at contact depths below 55 nm (see figures 6 and 7) also confirmed the presence of the oxide layer. For the depth profile below 10 nm, there was an increase in oxygen concen-

Table 3.
Al390-T6 alloy composition.

Element	Al	Si	Fe	Cu	Ti	Mn	Mg	Cr	Ni
Specified Weight %	Balance	16–18	0.5	4–5	—	0.1	0.45–0.65	—	—

tration from 3% at $t = 0$ min (virgin) to 10% at $t = 10$ min and finally to 20% at $t = 25$ min at 200 nm below the surface, which suggested that the longer the time the disk was tested in the presence of CO_2 refrigerant, the higher the oxygen concentration found in the topmost surface layer. Similar behavior was observed with the evolution of carbon concentration.

Furthermore, progressive burnishing experienced by the disk surface in the presence of CO_2 refrigerant gave rise to higher silicon concentration. Shown in figure 9(b) is the AES data of silicon concentration for all samples versus depth below the surface. The silicon concentration steadily increased from 3% in the virgin sample to 20–25% in sample C ($t = 22$ min) while it was reduced to almost the virgin level in sample D ($t = 25$ min). This was different from previous studies under starved lubrication conditions using POE lubricant and R410a refrigerant, which showed steady depletion of silicon as the disk went through the different stages of wear intensity until scuffing [1,15]. In both cases, with tribological testing and the local heating of the asperities, silicon segregates from the aluminum matrix and in the earlier study with R410a, the absence of oxygen allowed the silicon to deplete from the sample thus weakening the topmost layer [1,15]. In the current work with CO_2, the abundance of oxygen reacts with segregated silicon to form oxides, thus the strengthening of the topmost surface layer, as seen in figure 7. Note however, that in this study the level of silicon concentration reduced to that of the virgin sample at the end of the transient stage ($t = 25$ min). This trend of silicon concentration was in agreement with the trend observed in hardness as shown in figure 7, where the silicon concentration and hardness increased accordingly in the initial stages of the experiments. Similarly, the decrease in hardness at the final stage corresponds to the decrease in silicon concentration. Since silicon has high hardness, the silicon concentration plotted in figure 9(b) was consistent with the surface hardening and weakening as determined by the nanoindentation.

Note that the AES analysis presented above was performed on the samples that were exposed to the atmosphere after testing, i.e., in taking them from the HPT to the AES. Nevertheless, the data shown in figures 8 and 9 clearly show that this exposure had an insignificant effect on the 200 nm thick surface layer that was drastically changed during tribological testing.

5. 2-D surface roughness analysis

5.1. Background

As the mechanical and chemical analyses were able to reveal important changes in the surface properties experienced during the evolutionary stages of the submerged tribological experiments, topographical analysis can also be used to quantify the geometric changes associated with surface burnishing. In recent work by Suh *et al*. [16], roughness parameters were successfully applied to describe quantitatively the change in the disk surface topography as an indicator or pre-cursor to the scuffing process. In this part of the work, the primary 2-D parameter set [17] was used to investigate the surface changes occurred with progressively longer tribological experiments. A total of 15 roughness descriptors describe the geometric properties of a given surface, including amplitude, spatial and hybrid parameters along with volumetric aspects of lubricant retention capabilities of the surface roughness. Since the wear mechanism changes not only the geometrical properties of the surface, but also its functional properties such as fluid retention properties, mechanical resistance and load carrying capacity, functional parameters may be particularly useful in submerged lubrication conditions.

An optical surface profiler was used to measure the surface topography and the image dimensions of each surface were approximately 1.2 mm by 0.9 mm. To preserve statistical variation within each sample, three measurements were performed at different locations in both virgin and worn parts. These image data were then processed to extract the 15 roughness

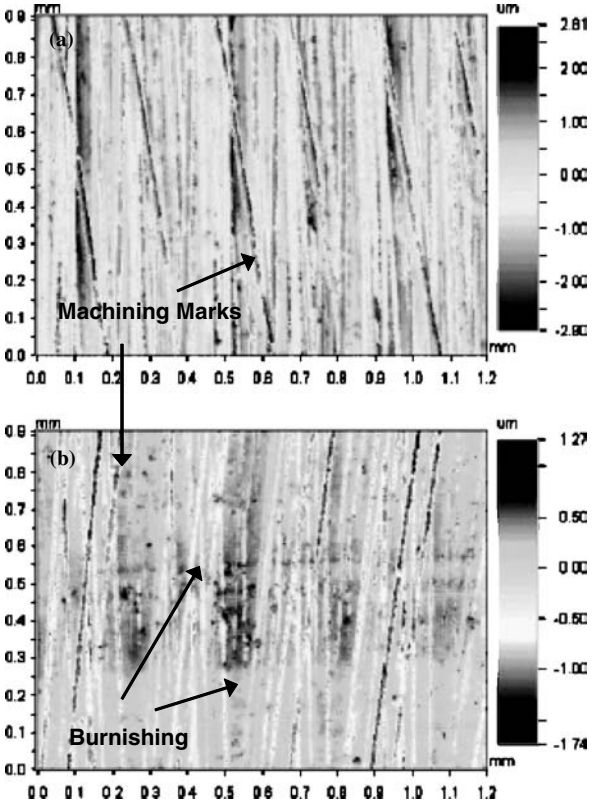

Figure 10. 2-D roughness images of A1390-T6 disks: (a) virgin, (b) sample C ($t = 22$ min).

descriptors specified in the primary 2-D parameter set. Figure 10(a) and (b) show topographical images of the Al390-T6 disks at virgin stage and after 22 min of tribological testing (sample C), respectively. Figure 10(b) shows traces of sliding in the horizontal direction, similar to what was shown in the SEM image in figure 5. Note that the dominant lay direction shown in both figures 10(a) and (b) was due to the machining marks with the direction of sliding approximately perpendicular to this texturing. In order to minimize the disk-to-disk variation in the original virgin disks the same methodology was adopted as in the work by Suh *et al.* [16], where the virgin part was directly compared to the worn counterpart within the same sample.

5.2. Results and discussion

Amplitude parameters give the scalar measure of vertical variation of surface roughness and they are the simplest parameters to describe surface burnishing. Table 4 lists some of the amplitude parameters from the 2-D primary roughness set, namely, the RMS deviation (S_q), skewness (S_{sk}) and kurtosis (S_{ku}) values for the Al390-T6 disk surfaces at different tribological stages. The virgin and mildly-worn states are denoted as V and W, respectively, and % refers to corresponding percent change from V to W. Note that the values listed in table 4 are the statistical average of three different measurements made for each sample.

The overall trends established in the center-line-average (S_a) and the RMS deviation S_q values were similar despite the inherent disk-to-disk variation. For example, as the surface was progressively burnished from virgin to mildly worn state, the percent change in S_q values increased from 11.6% at virgin to 37.5% at $t = 22$ min. At $t = 25$ min, however, the percent change in S_q values decreased to 10.5%.

As shown in figure 11(a), the disk surfaces also became more negatively skewed as the disk surface underwent tribological testing. Negligible percent change in skewness at $t = 10$ min, however, implied that the amplitude variation did not change notably at this stage. This can be attributed to the relatively low load applied initially, resulting in less asperity contacts as quantified by the small friction coefficient shown in figure 2. Referring to table 4, the virgin surfaces were already negatively skewed and became even more so as burnishing progressed further. The kurtosis (S_{ku}) also displayed a similar trend (not shown). The percent change in skewness and kurtosis values between virgin and worn state seemed to decrease after $t = 22$ min, indicating a sudden change of geometric characteristics at the final evolutionary stage.

The roughness variation in the planar direction as determined by the burnishing can be described by spatial parameters. The density of summits (S_{ds}), degree of texture isotropy (S_{tr}) and the direction of dominant surface lay (e.g., machining marks and burnishing direction) can all be represented by the spatial parameters. As summarized in table 4, the percent change in the density of summits (S_{ds}) from virgin to worn state increased with successive test up to $t = 22$ min. The progressive increase in S_{ds} values can be explained by the smoothening of top asperities exposing more asperities in the lower region to the environment, thereby increasing the total number of summits. However, the increasing trend in S_{ds} was reversed at $t = 25$ min, which is consistent with the trends displayed by the amplitude parameters.

Hybrid parameters can be used to describe the combined geometric characteristics of amplitude and spatial variations as a result of burnishing. Depicted in

Table 4.
2-D Primary roughness parameters for samples undergoing tribological testing.

2-D Primary Roughness Parameters			A (10 min)	B (20 min)	C (22 min)	D (25 min)
(Amplitude Property)	S_q	V	0.760	0.813	0.616	0.522
• RMS (μm)		W	0.672	0.646	0.385	0.467
		%	−11.6	−20.5	−37.5	−10.5
(Amplitude Property)	S_{sk}	V	−0.399	−0.272	−0.477	−0.264
• Skewness (unitless)		W	−0.424	−1.206	−1.161	−0.613
		%	−6.3	−343.4	−143.4	−132.2
(Spatial Property)	S_{ds}	V	3349.4	3259.9	3404.6	3573.4
• Density of Summits ($\times 10^3$ mm^{-2})		W	3417.4	3923.3	4390.6	3795.3
		%	2.0	20.3	29.0	6.2
(Hybrid Property)	$1/S_{sc}$	V	30.31	28.63	33.35	32.78
• Mean Summit Radius (μm)		W	34.23	47.50	65.30	40.90
		%	12.9	65.9	95.8	24.8
(Functional Property)	S_{ci}	V	1.360	1.407	1.280	1.435
• Core Fluid Retention Index		W	1.336	0.831	0.940	1.302
(e.g., Gaussian = 1.56)		%	−1.8	−40.9	−26.6	−9.3

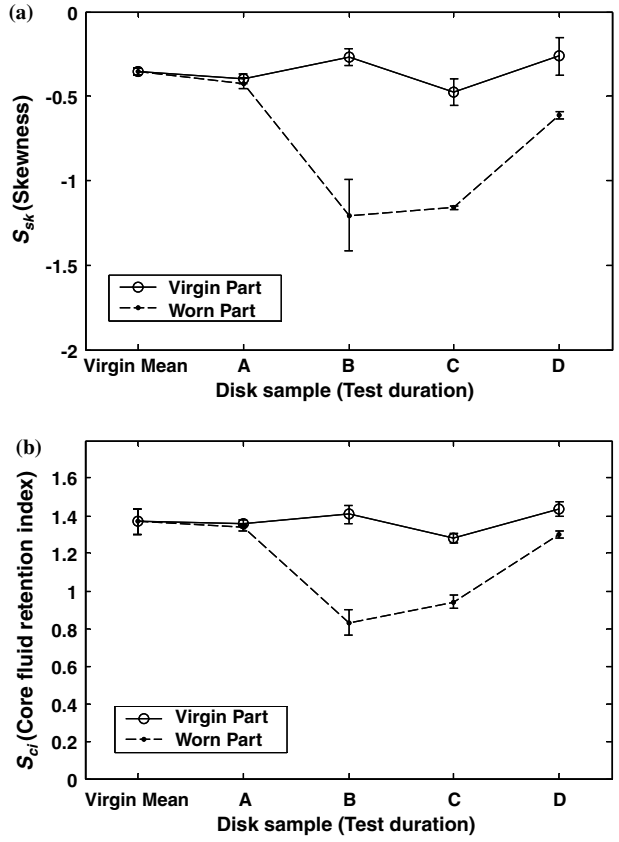

Figure 11. (a) Mean skewness variation and (b) mean core fluid retention index variation with different levels of tribological testing (error bars indicate ± 1 standard deviation).

table 4 is one of the hybrid parameters analyzed in this study; the inverse of the mean summit curvature or S_{sc}^{-1}, which is equivalent to the mean summit radius. The mean summit radii in the worn surfaces were always larger than those in the virgin surfaces, and the percent change generally increased with successive burnishing with the exception of $t = 25$ min. Increasing mean radius of the surface asperities up to $t = 22$ min suggested smoothening surface due to mild burnishing. The decreased percent change in S_{sc}^{-1} at $t = 25$ min, however, indicates less smoothening of the asperities at this tribological stage.

The functional parameters are normalized indices essentially derived from 2-D bearing area curves [16,17]. In general, core fluid retention index (S_{ci}) decreases as wear progresses thus it can be an indicator to the change in lubrication retention property of the surface as it undergoes stages of progressive tribological testing. Since these were fully submerged lubricated tests, only S_{ci} was included in table 4 and also depicted in figure 11(b). Small change in S_{ci} observed at $t = 10$ min was similarly observed in other roughness parameters such as the skewness trend. This implied that while the mechanical and chemical properties of the topmost surface changed at $t = 10$ min, the geometrical property was not significantly affected. Although the core fluid retention indices for the worn surfaces were always lower than the virgin counterparts, the percent change did not increase linearly with testing duration. Interestingly, the percent change at $t = 25$ min seemed to be smaller than the two previous stages. This suggested that a significant change in the disk roughness had occurred after 22 min which seemed to affect the lubrication retention property of the disk.

The analyses of the amplitude and spatial parameters showed that longer tribological tests led the disk surfaces to be mildly-worn or burnished in the early stages of tribological experiments. Most of the calculated parameters, however, displayed decreasing trends in percent change at $t = 25$ min, indicating its tendency towards the steady-state after the transient tribological behavior. Also, some of the roughness parameters could be utilized as successful indicators to surface burnishing. This change in roughness parameter trends at the end of the transient stages coincided with the behaviors observed in both mechanical (section 3) and chemical analyses (section 4). The behavior of the surface roughness during the transient stage combined with the mechanical and chemical behaviors of the topmost surface imply that after a prolonged testing duration, the steady-state is reached.

6. Conclusion

Tribological tests have been performed for a pin-on-disk contact interface between 52100 steel pins and Al390-T6 disks under submerged lubricated conditions using different combinations of refrigerants and lubricants. Although scuffing or severe wear were not observed as in starved lubrication conditions, mild wear or burnishing on the disk surfaces was observed which indicated asperity contacts due to the breaking of the EHL film separating the surfaces. It was found that CO_2 performs better than a conventional refrigerant R410a when used with PAG and POE lubricants. Detailed experiments were then conducted under CO_2/PAG environment as a means to study the evolution of the tribological interface during sliding contact. Subsequently, nanohardness measurements were performed using nanoindentation at contact depths ranging from 5 nm to 200 nm. It was observed that the material on the top 200 nm surface layer hardened initially but weakened toward the end of the transient testing stages. It was also confirmed that the hardness of topmost surface layers is closely related to the silicon and oxygen concentrations in this layer. Combination of the mechanical and chemical analyses suggested that the surface approached steady-state near the end of a transient tribological stage. Detailed examinations of various roughness parameters further verified that the surfaces experienced mild burnishing

during the transient stages of tribological behavior. The complex evolutionary process which involves mechanical, chemical and topographical interactions on the topmost surface layer depends on the initial operating parameters of the tests. Their interaction can determine successful operation of the device as steady-state EHL regime is reached.

Acknowledgments

This research was supported in part by the National Science Foundation and the 30 member companies of the Air Conditioning and Refrigeration Center, and Industry University Cooperative Research Center at the University of Illinois at Urbana-Champaign. The chemical analyses and mechanical property measurements were performed at the Center for Microanalysis of Materials at the University of Illinois, which is supported by the U.S. Department of Energy under Grant DEFG02-96-ER45439. The authors gratefully acknowledge these supports.

References

[1] S.R. Pergande, A.A. Polycarpou and T.F. Conry, J. Trib. 126 (2004) 573.
[2] T. Sheiretov, H.K.Yoon and C. Cusano, Trib. Trans. 41 (1998) 435.
[3] H.K. Yoon, T. Sheiretov and C. Cusano, Wear 237 (2000) 163.
[4] E.C. Cutiongco and Y.W. Chung, Trib. Trans. 37 (1994) 622.
[5] J.A. Williams, *Engineering Tribology* (Oxford, New York, 1994).
[6] G. Lorentzen, Int. J. of Refrig. 18 (1995) 190.
[7] C. Seeton, J. Fahl and D. Henderson, *Proceedings of the 4th IIR-Gustav Lorentzen Conference on Natural Working Fluids at Purdue* (2000) 417.
[8] Daphne Hermetic *"End-Capped" PAG Lubricants Manual* (IDEMITSU: Apollo America Corporation).
[9] H. Li, K.C. Lilje and M.C. Watson, Int. Compressor Eng. Conf. (2002).
[10] W.C. Oliver and G.M. Pharr, J. Mater. Res. 7 (1992) 1564.
[11] W. Lu and K. Komvopoulos, J. Appl. Phys. 85 (1999) 2642.
[12] N. Yu, A. Polycarpou and T. Conry, Thin Solid Films 450 (2004) 295.
[13] R.E. Walpole, R.H. Myers and S.L. Myers, *Probability and Statistics for Engineers and Scientists* (Prentice Hall, New Jersey, 1998).
[14] *Metal Handbook* 9th edn. Vol. 10 Materials Characterization, eds. R.E. Whan (American Society for Metals, 1986).
[15] J.J. Patel, *Investigation of the Scuffing Mechanism under Starved Lubrication Conditions Using Macro, Meso, Micro and Nano Analytical Techniques* (M.S. Thesis, Univ. of Ill. at U-C, 2000).
[16] A.Y. Suh, A.A. Polycarpou and T.F. Conry, Wear 255 (2003) 556.
[17] K.J. Stout, P.J. Sullivan, W.P. Dong, E. Mainsah, N. Luo, T. Mathia and H. Zahouani, *The Development of Methods for the Characterization of Roughness in Three Dimensions* (Commission of the European Communities, Brussels-Luxembourg, 1993).